Europace (2005) 7, S93–S104

ELSEVIER

EUROPEAN SOCIETY OF CARDIOLOGY®

Alternating conduction in the ischaemic border zone as precursor of reentrant arrhythmias: A simulation study

Olivier Bernus [a,*], Christian W. Zemlin [a], Roman M. Zaritsky [b], Sergey F. Mironov [a], Arkady M. Pertsov [a]

[a] *Department of Pharmacology, SUNY Upstate Medical University, 750 East Adams Street (WHA) Syracuse, NY 13210, USA*
[b] *Computer Science Department, Montclair State University, Upper Montclair, NJ 07043, USA*

Submitted 21 January 2005, and accepted after revision 3 May 2005

KEYWORDS
acute regional ischaemia;
2:1 conduction blocks;
APD and T-wave alternans;
reentry

Abstract **Aims** Here, we investigate the mechanisms underlying the onset of conduction-related arrhythmias in a three-dimensional (3D) computational model of acute regional ischaemia.
Methods Ischaemia was introduced by realistic gradients of potassium, pH, oxygen and electrical coupling in a 3D slab of ventricular tissue using the LRd model. We focused on a specific stage (10–15 min after occlusion) at which an intramural non-conductive ischaemic core (IC) surrounded by a border zone (BZ) has formed.
Results At pacing frequencies greater than 4.5 Hz, we observed narrow areas (0.5 mm wide) of 2:1 conduction blocks at the periphery of the IC. As the pacing frequency increased, the area of block widened to 9 mm and gave rise to reentry at the periphery of the BZ. Alternating conduction blocks produced discordant action potential duration (APD) alternans throughout the slab and T-wave alternans in pseudo-ECG. Slowing the recovery of the calcium current broadened the range of pacing frequencies at which blocks were observed. Hyperkalaemia alone was sufficient to induce the alternating blocks.
Conclusion Computer modelling predicts that ischaemia-related arrhythmias are triggered by calcium-mediated alternating conduction blocks in the ischaemic border zone. Alternating conduction blocks lead to intramural reentry and APD alternans.

* Corresponding author. Tel.: +1 315 464 5141; fax: +1 315 464 8014.
E-mail address: bernuso@upstate.edu (O. Bernus).

1099-5129/$30
doi:10.1016/j.eupc.2005.03.018

Introduction

Cardiac death remains the leading cause of mortality in the industrialized world [1—3]. Ventricular arrhythmias, ventricular fibrillation (VF) in particular, are the major cause of sudden cardiac death [3]. There is compelling clinical evidence that acute myocardial ischaemia is one of the most important causes of ventricular arrhythmias in humans [4].

The onset of ischaemia-related arrhythmias occurs rapidly after coronary occlusion [4—6] and they are usually associated with T-wave alternans [7—11], which has been found to be a strong marker for electrical instability leading to sudden cardiac death [12—14]. It has been hypothesized that T-wave alternans is due to repolarization or action potential duration (APD) alternans at the single cell level [12,15,16]. In normal tissue it has been shown that APD alternans can lead to conduction blocks and multiple reentry [12,17,18]. In ischaemic tissue, however, the mechanisms linking APD and T-wave alternans to arrhythmias are less well understood.

In the present study we use mathematical modelling to investigate possible ionic mechanisms underlying the onset of ischaemia-related arrhythmias and their link to APD alternans. We construct a three-dimensional computational model of a slab of cardiac tissue. We focus on 10—15 min regional ischaemia after which a non-conductive ischaemic core (IC) has formed surrounded by an ischaemic border zone (BZ) with decreased excitability [19—21]. The excitable properties of the tissue are described by the dynamic Luo-Rudy model [22,23]. Acute ischaemia is modelled through its major pathophysiological components: elevated extracellular potassium concentration, acidosis, anoxia and electrical uncoupling.

Methods

Basic ventricular cell model

To represent the excitable dynamics of normal cardiac tissue, we used the dynamic Luo-Rudy model (LRd) developed by Faber and Rudy [22]. The LRd model is a general mammalian ventricular cell model, mainly based on data obtained from the guinea pig. The model includes different ionic channel currents, as well as ionic pumps and exchangers, and describes intracellular changes in ionic concentrations. Faber and Rudy introduced some changes in the calcium induced calcium release and in the sodium—calcium exchanger. Moreover, they formulated the Na^+-activated K^+ current, used to model the cell behaviour under Na^+ overload conditions at high pacing frequencies.

Ischaemic ventricular cell model

We have followed the approach of Shaw and Rudy [23] to model the three main components of ischaemia at the cellular level: hyperkalaemia, acidosis and anoxia. Hyperkalaemia was obtained by increasing the extracellular potassium concentration $[K^+]_o$. The effects of acidosis were modelled through a decrease in the sodium and L-type calcium channel conductances, g_{Na} and g_{Ca}, respectively, and through a shift $V_{s,Na}$ in the voltage-dependent kinetics of the sodium current. We mimicked anoxia by reducing the intracellular ATP concentration, which affects the ATP-dependent potassium and calcium channels.

Three-dimensional model of acute regional ischaemia

We considered three-dimensional slabs of cardiac tissue of 37 mm × 37 mm × 7.4 mm. We modelled the electrical properties of the tissue using the monodomain approach. The components of the conductivity tensor were determined using the same approach as Panfilov and Keener [24] for uniform fibre rotation of 120° from endo- to epicardium. We investigated several ranges for the fibre orientation going from [0°,120°] to [180°,400°]. The first value denotes the angle of the fibres on the endocardium, and the second value denotes the angle on the epicardium, with respect to the *x*-direction (see Fig. 1A). The model parameters were chosen to yield a longitudinal conduction velocity of 60 cm/s in normal tissue. The ratio of the conductivities along and across the fibres was set to 9, yielding action potentials propagating three times faster in the longitudinal than in the transverse direction.

We modelled an IC of size 9.25 mm × 37 mm × 1.85 mm at mid-depth in the tissue (see Fig. 1A). In this region we used parameter values typical of 10—15 min ischaemia: [23] $[K^+]_o = 14.5$ mM, $[ATP]_i = 3$ μM, $V_{s,Na} = 3.4$ mV, and we reduced the conductances g_{Na} and g_{Ca} by 25%. The ischaemic core was surrounded by an ischaemic BZ spanning a volume of 18.5 mm × 37 mm × 5.5 mm, including the core. In the ischaemic border zone, we allowed all parameters to return to their normal values along a linear gradient (see Fig. 1B). In

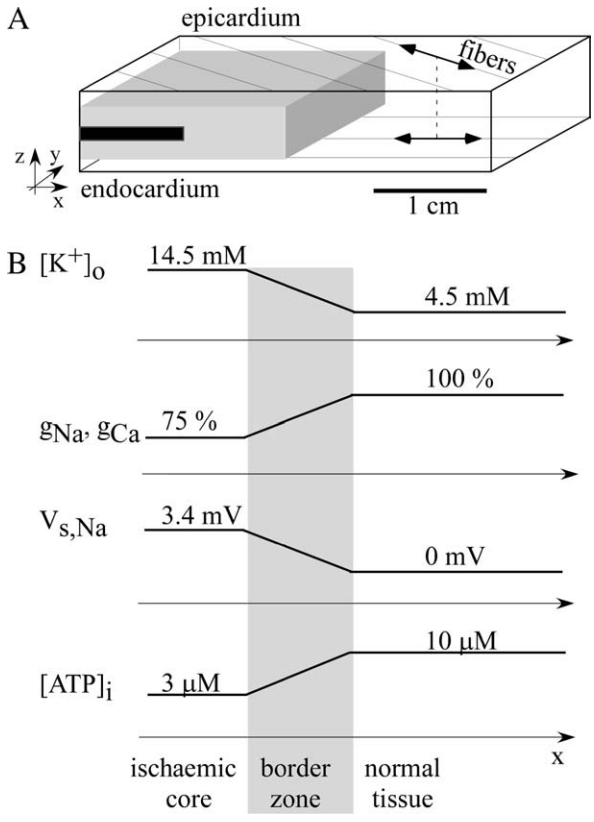

Figure 1 Three-dimensional model of acute regional ischaemia. (A) Slab of ventricular tissue of 37 mm × 37 mm × 7.4 mm, including an ischaemic core (black region), ischaemic border zone (grey region) and normal tissue (transparent). The fibre orientation is illustrated on the endo- and epicardial surfaces with arrows and thin solid lines. (B) Gradients of extracellular potassium $[K^+]_o$, sodium and calcium conductances g_{Na} and g_{Ca}, shift $V_{s,Na}$ in kinetics of the sodium current and intracellular ATP concentration, along the *x*-direction and through the ischaemic core.

some simulations we included partial electrical uncoupling [25,26], by reducing the conductivity by 50% in the ischaemic core and allowing it to return to 100% through the ischaemic BZ.

Pacing protocol

In our simulations we paced the entire endocardial (bottom) surface (Fig. 1) using an incremental pacing protocol to simulate rapid endocardial activation through the Purkinje network. The pacing frequency went from 2 Hz up to 10 Hz in steps of 0.2 Hz. All stimuli had an amplitude of twice threshold and lasted for 2 ms. For the chosen parameter values we obtained a non-conductive IC and an ischaemic BZ with decreased excitability.

Pseudo-electrocardiogram

We computed pseudo-electrocardiograms (ECG) during our simulations using the dipole approximation:

$$\mathrm{ECG} = \frac{\sum (\nabla V_m \times \mathbf{r})}{r^3} \quad (1)$$

Where the sum $\sum$ runs over all points of the slab, V_m is the membrane potential and **r** is the position vector of the point with respect to the electrode. We placed our electrode 3 cm above the middle of the epicardial surface.

Numerical approach

The monodomain cable equation was solved using a forward Euler scheme with a time step of 0.01 ms a space step of 0.185 mm, yielding a numerical accuracy of more than 90% with respect to the conduction velocity. The relaxation equations of the gating variables in the LRd model were integrated using a technique presented by Rush and Larsen [27]. All computations were carried out on a parallel cluster consisting of 16-nodes equipped with dual AMD Athlon MP 2200 + processors running at 1.8 Ghz. We used the MPI-library and a simple ''domain slicing'' algorithm to parallelize the C++ code [28]. A one s simulation took approximately 11 h 45 min of central processing unit time.

Results

Alternating conduction blocks in the ischaemic BZ

As the pacing frequency reached 4.5 Hz and increased further, we observed a gradually growing area close to the ischaemic core, showing conduction blocks on alternate beats. Fig. 2 illustrates these alternating propagation patterns in a transmural cross-section of the slab. Fig. 2A shows three consecutive beats when pacing at 8 Hz. During beats 1 and 3 the wave propagates through the BZ (dotted line) close to the ischaemic core (white box). During the second beat a portion of the ischaemic BZ in the vicinity of the core shows conduction failure. As a result, the wave detaches from the core and propagates around the area of conduction block (see arrow).

To quantify the size of the area showing alternating conduction block we measured the points of the slab where the transmembrane potential remained below −65 mV. Fig. 2B shows the area

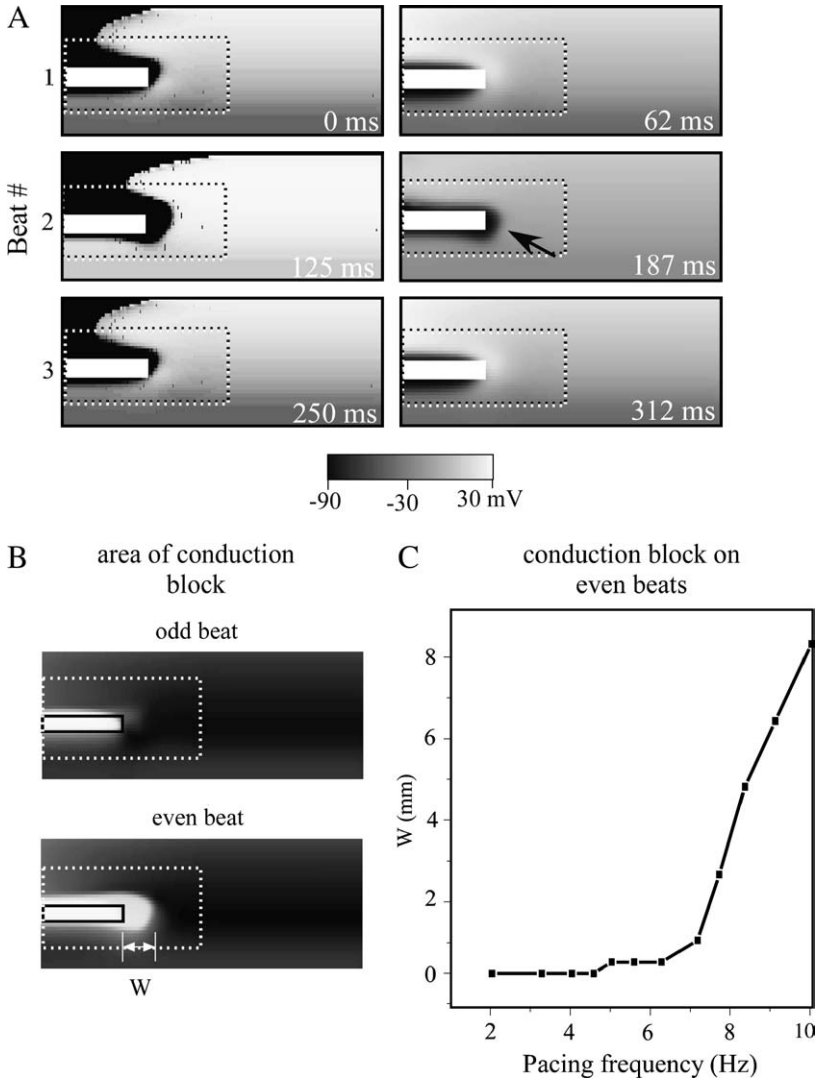

Figure 2 Alternating conduction blocks in the ischaemic border zone. (A) Snapshots of the propagating wave front for three consecutive beats at 8 Hz in a transmural cross-section of the slab. The ischaemic core is depicted as a white rectangle, while the border zone is delimited by a dotted line. Membrane potential is shown in a grey scale indicated at the bottom of the panel. The first and third beats propagate close to the ischaemic core, while the second beat surrounds an area larger than the ischaemic core. (B) The area of conduction block on odd and even beats is depicted in grey in a transmural cross-section of the slab. A solid line delimits the ischaemic core; a dotted line the ischaemic border zone. On odd beats the area of conduction block almost perfectly coincides with the ischaemic core, while on even beats a thin region around the ischaemic core also exhibits conduction block. (C) Width *W* of the area of conduction blocks on even beats as a function of the pacing frequency. *W* was measured at mid-depth in the tissue and at a cutoff level of 10% action potential amplitude (see panel A).

of conduction block for odd and even beats (white area). On odd beats the area exhibiting conduction block roughly corresponds to the IC. On even beats, however, conduction blocks developed as well in a layer surrounding the IC. We quantified the size of the area of conduction block on even beats by measuring its width *W* at mid-depth in the slab (see Fig. 2B). Fig. 2C shows the dependence of *W* on the pacing frequency. The initially narrow area showing conduction blocks rapidly expanded as the pacing frequency increased above 4.5 Hz and reached the whole width of the BZ (about 9 mm) at the end of the pacing sequence. Note that the area showing conduction block on odd beats also grew as a function of the pacing frequency (not shown). However, it always remained substantially smaller than the area of conduction block on even beats (e.g. less than 1 mm wide at 10 Hz, compared with almost 9 mm on even beats).

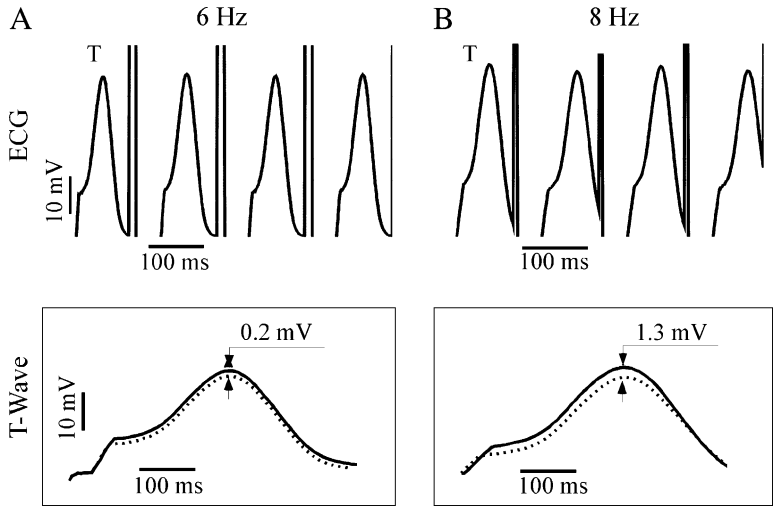

Figure 3 T-wave alternans: pseudo-ECGs recorded 3 cm above the epicardial surface, during pacing at 6 Hz (A) and 8 Hz (B). The insets show a superposition of two consecutive T-waves, illustrating T-wave alternans. The amplitude of T-wave alternans is about 0.2 mV for a pacing frequency of 6 Hz (A) and is about 1.3 mV for a pacing frequency of 8 Hz (B).

T-wave alternans

The development of alternating conduction blocks coincided with the development of microvolt level T-wave alternans in the pseudo-electrocardiograms. The amplitude of T-wave alternans increased with increasing pacing frequency. Fig. 3A,B shows the computed ECG when pacing at 6 and 8 Hz, respectively. The insets show a comparison between two consecutive T-waves. The amplitude of the T-wave alternans was about 0.2 mV for the pacing frequency of 6 Hz (see bottom panels). When we paced the endocardial surface at 8 Hz, we observed a T-wave alternans amplitude of about 1.3 mV (see inset in Fig. 3B). At the end of our pacing sequence, the amplitude of the T-wave alternans reached 10 mV (not shown). The amplitude of the T-wave alternans correlates with the size of the area showing 2:1 conduction blocks (Fig. 2C).

APD alternans

The underlying mechanism for T-wave alternans was APD alternans (see Fig. 4). Fig. 4A shows the effect on repolarization for the three beats shown in Fig. 2. The white arrow indicates the area close to the ischaemic core where alternations in repolarization were observed: long APD on odd beats and short APD on even beats.

At pacing frequencies greater than 8 Hz, APD alternans became discordant or ''out-of-phase'' in different regions of the slab of ventricular tissue. Fig. 4B shows action potential recordings in four different locations of the slab. In the ischaemic border zone we observed long APDs on odd beats and short APDs on even beats (L-S-L sequence), as shown by the action potential recordings in sites a and b (upper two traces in panel B). Note that, close enough to the ischaemic core we had 2:1 responses, with full action potentials on odd beats and supra-threshold activity on even beats (site a). In the region of normal tissue located right above the ischaemic area (site c), we observed alternans with an opposite phase: short APDs on odd beats and long APDs on even beats (S-L-S sequence). Arrows between the second and third trace indicate corresponding action potentials. In the remaining parts of the slab no alternans was observed (site d). Fig. 4C schematically represents the phase of alternans in the different parts of the slab: no alternans in the dotted region, L-S-L alternans in the crosshatched region, which corresponds to the ischaemic BZ, and S-L-S alternans in the hatched area. The spatial distribution of the phase of alternans is readily explained by noting that short APDs in the BZ on even beats are associated with conduction delays and blocks in the BZ. This results in an increase in the diastolic interval in the upper part of the slab and, hence, in longer APDs. The opposite is true on odd beats.

Single cell simulations

To determine whether T-wave and discordant alternans were caused by repolarization alternans at the single cell level or occurred secondary to the alternating conduction blocks, we simulated

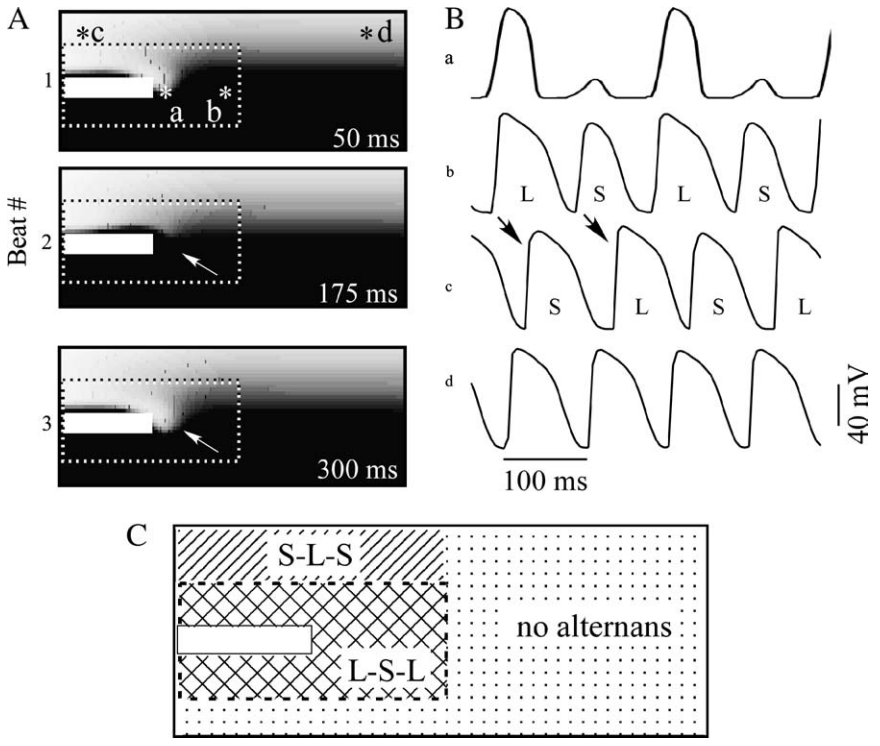

Figure 4 Discordant APD alternans throughout the slab. (A) Snapshots of the wave tail of three consecutive beats at 8 Hz in a transmural cross-section of the slab. The ischaemic core is depicted as a white rectangle, while the border zone is delimited by the dotted line. Membrane potential is shown in a grey scale indicated at the bottom. APD alternans is observed close to the ischaemic core (indicated by white arrows). (B) Action potential recordings in four locations of the slab indicated in panel A (beat 1). In the ischaemic border zone we observed a long-short-long (L-S-L) sequence (locations a and b), whereas in location c a short-long-short sequence (S-L-S) was found. No APD alternans was detected in normal tissue at location d. (C) Schematic representation of the phase of alternans in the different parts of the slab: no alternans in the dotted region, L-S-L alternans in the crosshatched region and S-L-S alternans in the hatched region.

single cells from three different locations in the ischaemic BZ: 2.5, 5 and 7.5 mm from the ischaemic core at mid-depth in the tissue. We applied our pacing protocol in those single cells and recorded the action potentials. Fig. 5 summarizes our results. Fig. 5A shows action potential recordings (solid line) when pacing the three single cells from different locations (see transmural cross-section on the left) at 10 Hz. The APD measured at 90% of repolarization is indicated for each action potential in milliseconds. For cells isolated from the region close to the IC (upper trace) only a small APD alternans of about 2 ms could be observed. Further away from the core (two lower traces) APD alternans was even smaller. For comparison, we show the action potential recordings obtained in the same location and at the same moment during the pacing protocol, in the three-dimensional simulation (dashed line). These recordings are substantially different from the single cell measurements, as 2:1 responses were observed in the two upper traces and an APD alternans of about 20 ms was found in the third location (lower trace). Fig. 5B shows the dependence of APD on the pacing frequency in the point corresponding to the upper trace in Fig. 5A. Again, we compare the results obtained in single cells (solid line) with those in the three-dimensional tissue (dashed line). At the single cell level, we observed APD alternans ranging from 1 ms at 8 Hz to 2 ms at 10 Hz. In the three-dimensional simulation small APD alternans of about 1 ms was observed at frequencies as low as 6 Hz. It rapidly grew to more than 10 ms for pacing frequencies of 7.5 Hz. For greater pacing frequencies we obtained a 2:1 responses.

The major differences between the single cell and three-dimensional simulations illustrated by Fig. 5, led to the conclusion that repolarization alternans cannot explain the observed APD and T-wave alternans. Hence, our attention turned to the depolarization phase and the ionic currents responsible for propagation in highly depressed tissue.

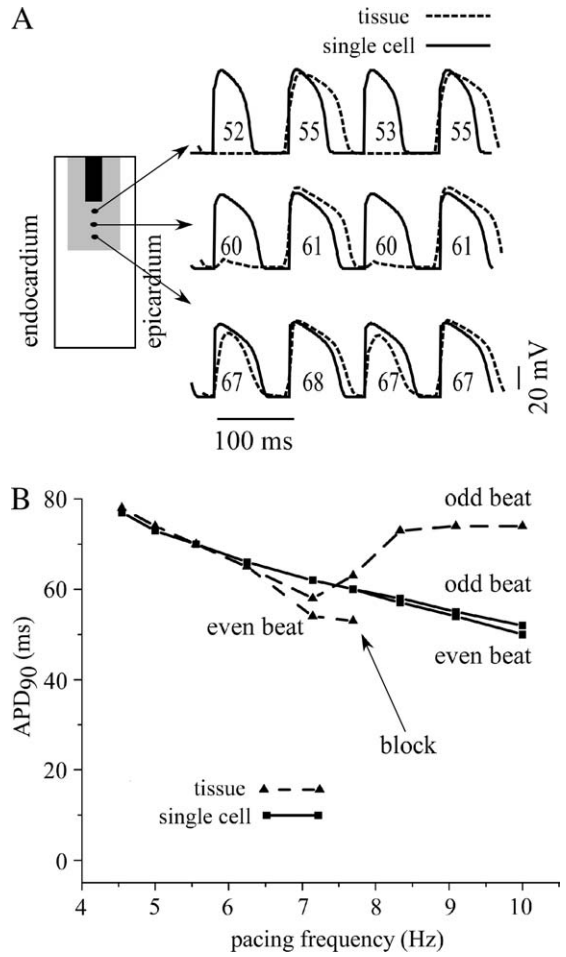

Figure 5 Comparison of APD alternans in single cells and tissue. (A) Action potential recordings at 10 Hz pacing frequency in single cells (solid lines) ''isolated'' from the ischaemic border zone at distances of 2.5, 5 and 7 mm, respectively, from the ischaemic core. The APD of each action potential measured at 90% of repolarization is indicated. The dashed lines show action potentials from the same locations and at the same pacing frequency, but recorded in the three-dimensional tissue. APD alternans was more pronounced in the tissue than in the single cells. (B) Dependence of APD on the pacing frequency at 2.5 mm from the ischaemic core (upper trace in panel A). Results obtained in the single cell simulation (solid lines + squares) are compared with those in the three-dimensional tissue (dashed lines + triangles). In the three-dimensional tissue an earlier onset and a larger amplitude of APD alternans is observed.

Ionic mechanisms

We investigated the availability of the currents that were shown to play a role in propagation through areas of reduced excitability due to ischaemia: the sodium current and the L-type calcium current [30]. Availability of these currents heavily depends on how much their inactivation and reactivation variables have recovered from the preceding action potential. In the Luo-Rudy model, the in- and reactivation of the sodium current are described by two voltage-dependent gating variables, h and j. The inactivation of the L-type calcium current is regulated by a voltage-dependent gating variable f and a calcium-dependent gating variable f_{Ca}.

Fig. 6 shows the time course of the sodium and calcium in- and reactivation variables in the ischaemic BZ for three beats at 8 Hz. Fig. 6A shows the product of h and j during those three beats. Close to the IC (site a in Fig. 3) there is almost no sodium current available as $h \times j$ is always below 0.05. The availability of the sodium current gradually increased away from the IC. For comparison, we show the time evolution of $h \times j$ in normal tissue (site d in Fig. 3). In this region, $h \times j$ recovers to 0.9 at the onset of each action potential. The 2:1 conduction blocks originate in the immediate vicinity of the ischaemic core, where no sodium current is available. The alternating conduction blocks should therefore be related to the inactivation kinetics of the L-type calcium current, which are shown in Fig. 6B for f, and panel C for f_{Ca}. The voltage-dependent gating variable f alternates between the values of 0.92 at the onset of beats 1 and 3 and 0.8 at the onset of beat 2. The calcium-dependent variable f_{Ca} shows smaller alternations between the values of 0.64 and 0.62.

Both inactivation variables of the L-type calcium current show alternans. In order to identify whether the voltage-dependent or the calcium-dependent properties play the most important role in the conduction success or failure, we changed their kinetics separately by: (1) fixing the intracellular calcium concentration to constant values, resulting in a constant f_{Ca}, and (2) slowing the kinetics of the f gate by increasing its inactivation time constant τ_f to 300 ms for membrane potentials below 0 mV. The effects of these modifications on the occurrence of the 2:1 conduction blocks are presented in Fig. 7. Fig. 7A shows the width W of the area displaying 2:1 conduction blocks (see Fig. 2) in the control case (squares) and in two other cases where the intracellular calcium concentration was kept constant at 400 nM (circles) or at 600 nM (triangles). These values were chosen to yield APDs comparable with the control case. As can be inferred from this figure, the intracellular calcium cycling (or the lack of such cycling) has little effect on the occurrence of the 2:1 conduction blocks. Fig. 7B shows a comparison between control (squares) and slowed f gate kinetics

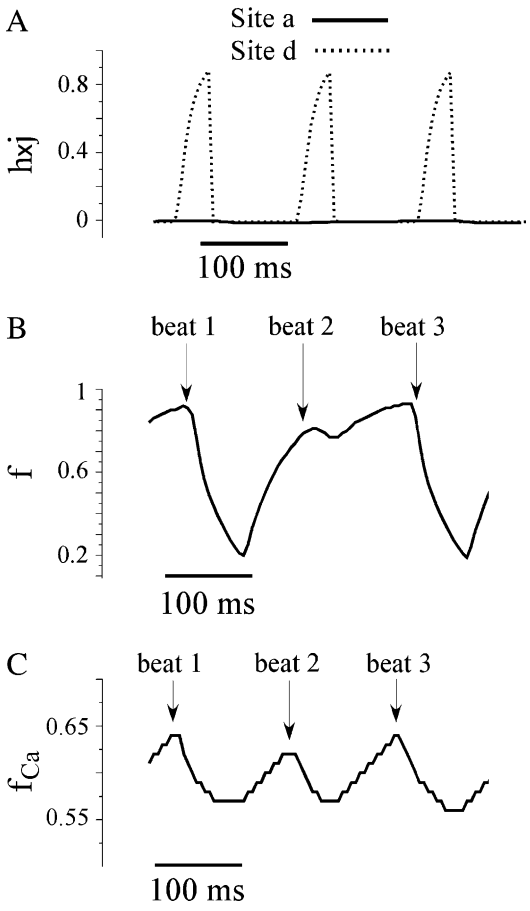

Figure 6 The inactivation and reactivation variables of the sodium (h and j) and calcium (f and f_{Ca}) current during three consecutive beats at 8 Hz. (A) Product of h and j close to the ischaemic core (solid line) and in normal tissue (dotted line). Close to the ischaemic core (site a in Fig. 3) the sodium current is almost completely inactivated as $h \times j < 0.05$. In normal tissue, the sodium current is available for each new beat as $h \times j$ recovers to 0.9 at the onset of each action potential. (B) Alternans of the voltage-dependent inactivation variable f close to the ischaemic core (site a in Fig. 3). (C) Alternans of the calcium-dependent inactivation variable f_{Ca} close to the ischaemic core (site a in Fig. 3).

(circles). The latter had a major effect on the alternating conduction blocks: they occupied a substantially larger area at lower pacing frequencies and eventually led to reentry at 9 Hz (last point on the curve) instead of 10 Hz in the control case (see below). These results show that the voltage-dependent recovery of the L-type calcium current plays an important role in the observed rate-dependent 2:1 conduction blocks.

Hyperkalaemia, acidosis and anoxia

We investigated which of these three components of ischaemia was responsible for the occurrence of the alternating conduction blocks in the ischaemic BZ. Therefore, we repeated our simulations for each component separately. In the case of regional acidosis or regional anoxia, we found no alternating conduction blocks in the studied range of pacing frequencies (not shown). However, they were observed in the model of regional hyperkalaemia. Fig. 7C shows a comparison of the width of the area showing 2:1 conduction blocks between the ischaemic model (squares) and the hyperkalaemic model (circles). The curves show an almost perfect match.

Effect of electrical uncoupling

Several studies have shown that after 15—20 min of acute ischaemia electrical uncoupling occurs between the cells [25,26]. It will affect the conduction velocity and is believed to play an important role in the arrhythmogenesis [31]. We investigated the effect of electrical uncoupling in our simulations by decreasing the conductivity between cells, both in the longitudinal and transverse direction. In the ischaemic core the conductivity was decreased to 50% of its normal value and it gradually increased to 100% along a linear gradient in the ischaemic BZ. Fig. 7C shows the effect of this partial uncoupling on the alternating conduction blocks. Again, we compare the width of the area showing 2:1 conduction block between the ischaemic model (squares) and the ischaemic model with uncoupling (triangles). Alternating conduction blocks developed in both cases at a pacing frequency of $\sim$5 Hz and then gradually increased. We observed a slightly larger area of alternating conduction blocks in the uncoupled case, which can be explained by the even more impaired conduction. In general, both curves show the same qualitative behaviour, illustrating the minor effect of uncoupling on the observed arrhythmogenesis.

Discordant alternans and reentry

Discordant alternans eventually led to the formation of reentry, in accordance with earlier experimental and computational studies [12,18]. Fig. 8 shows sequential snapshots of the electrical activity at 25 ms intervals in a transmural cross-section. The first four frames (beat 1) show a wave propagating through the BZ close to the ischaemic core and disappearing on the epicardial surface. The subsequent wave (the last of our pacing protocol) initiated 100 ms after the first, fails to propagate into the BZ and breaks at the interface of normal and ischaemic tissue, creating a phase singularity

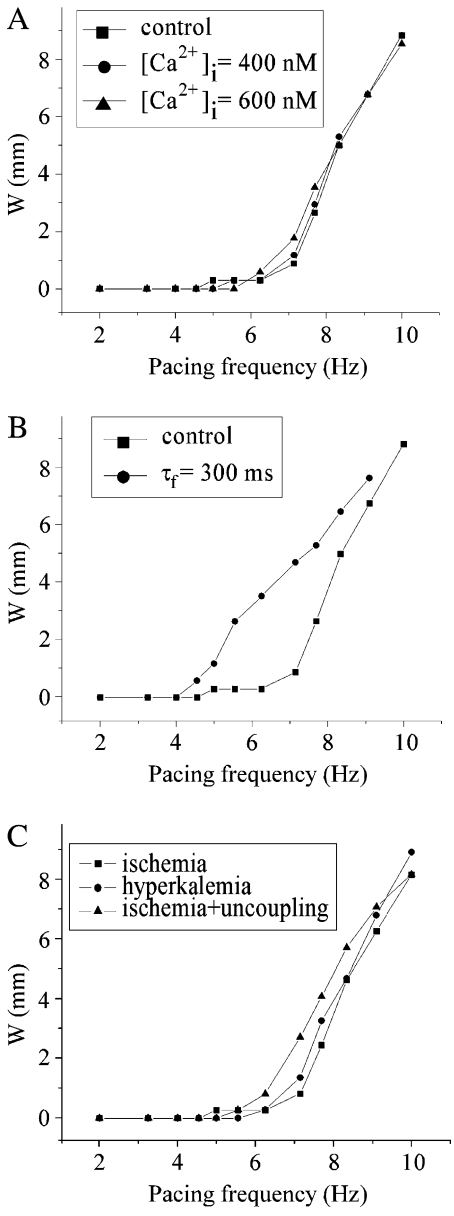

Figure 7 Effect of modifying the calcium current and role of selected components of ischaemia on *W* as a function of the pacing frequency. (A) Eliminating alternans of f_{Ca} by fixing the intracellular calcium concentration to a constant value (400 nM and 600 nM) has little effect on the occurrence of 2:1 conduction block. (B) Slowing down the voltage-dependent inactivation variable *f* by increasing its inactivation time τ_f to 300 ms below 0 mV results in an earlier onset and larger areas of 2:1 conduction block. (C) The role of hyperkalaemia and electrical uncoupling on the occurrence of 2:1 conduction blocks. Alternating conduction blocks were observed in a model of regional hyperkalaemia (no acidosis and anoxia). The width *W* showed the same dependence on the pacing frequency in the hyperkalaemic model (circles) and the full ischaemic model (squares). Incorporating partial uncoupling in the ischaemic region (see Methods for details) had only a minor effect on the occurrence of alternating conduction blocks (triangles).

S (black dot in a white circle). A few milliseconds later, the outer part of the BZ recovers excitability and the wave propagates towards the ischaemic core and back to the endocardial surface, leading to reentry. The first rotation of the wave after the end of the pacing sequence is shown in the last four frames. It involved propagation both through the normal and diseased tissue. The dynamics and life span of the reentrant wave were highly affected by the local fibre orientation. In our simulations, reentry lasted from two up to four rotations for different ranges of fibre angles (not shown). Reentry was reproducible in the model with only hyperkalaemia and in the ischaemic model including partial electrical uncoupling.

Discussion

T-wave alternans and APD alternans have been found to precede arrhythmias during acute ischaemia [7—9]. The mechanisms underlying alternans and the arrhythmogenesis during acute ischaemia remain, however, poorly understood. In the present study, we describe a possible novel mechanism for T-wave alternans and arrhythmias in a model of acute regional ischaemia: alternating conduction blocks in the ischaemic border zone. The observed 2:1 conduction blocks lead to discordant APD alternans throughout the tissue, which is in its turn responsible for T-wave alternans. Eventually, wave breaks occur and reentry is formed.

Simulated electrocardiograms were reminiscent of T-wave alternans, which has often been associated with repolarization alternans at the single cell level [29]. However, an experimental study performed by Downar et al. showed that during acute regional ischaemia 2:1 conduction block led to reentry, without any evidence for repolarization abnormalities [32]. Later, Smith and Cohen demonstrated, in a computational model, that T-wave alternans could be obtained through alternating conduction pathways arising from spatial heterogeneities in refractoriness [33]. Our simulations show that alternating conduction blocks in the BZ are the underlying mechanism for APD alternans leading to T-wave alternans, which can explain earlier experimental results [32]. The computations performed in single ischaemic cells excluded repolarization alternans as the underlying mechanism, thus favouring the hypothesis of conduction abnormalities. We investigated the ionic currents mediating propagation in the ischaemic border zone and found that conduction success or failure depends on the availability of the L-type calcium channel, through its voltage-dependent kinetics.

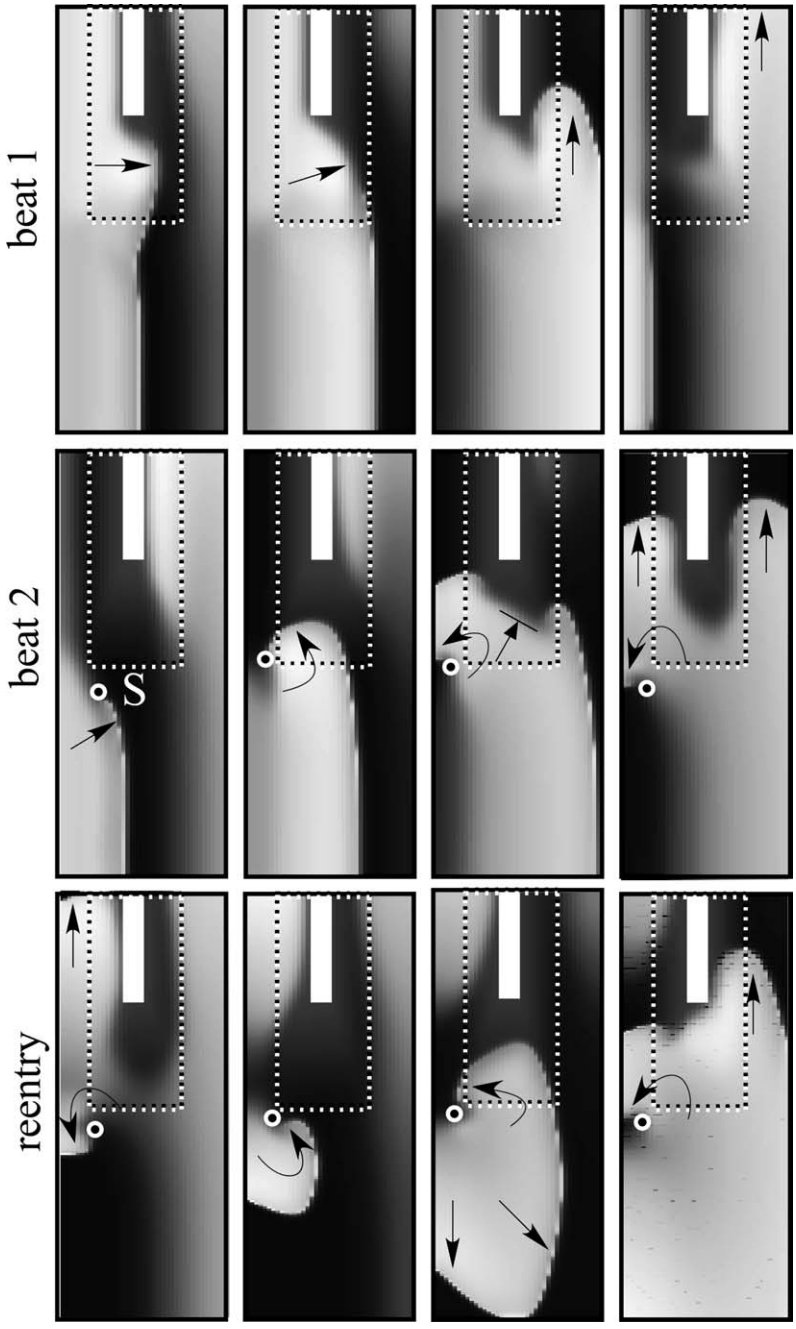

Figure 8 Intramural reentry as a result of alternating conduction block: snapshots of the electrical activity (25 ms interval) during the last two beats of the pacing sequence and resulting reentry. The grey scale for membrane potential is the same as in Figs. 2 and 3. During the first beat (four top panels) the wave propagates through the ischaemic border zone (delimited by a dotted line) close to the ischaemic core (white rectangle). The next wave (four middle panels) fails to propagate in the border zone and breaks at the boundary between ischaemic and normal tissue, creating a phase singularity S (black dot in white circle) leading to reentry. The first rotation of the reentrant wave is shown in the four bottom panels.

This result could potentially lead to new therapeutic targets during acute ischaemia.

Simulation studies performed by Shaw and Rudy highlighted the importance of the L-type calcium current in propagation through homogenous hyperkalaemic fibres [30]. In completely ischaemic fibres, i.e. including anoxia and acidosis, they found that calcium-supported conduction was more difficult to obtain. Later, Wang and Rudy showed in a computational model of a heterogeneous cable,

that the safety factor (SF) for propagation across a central hyperkalaemic part ($[K^+]_o = 14$ mM) was less than unity and that, therefore, propagation should fail [34]. Our findings may seem to contradict these previous results. However, this is not the case. The observations in our simulations are readily explained by the fact that even for SF < 1, action potentials can propagate decrementally over a few millimetre. In our model, the highly depressed areas within the intramural BZ were only a few millimetre thick, explaining the prominent role of the L-type calcium current in our study. Note that recently Ferrero et al. performed two-dimensional simulations of acute regional ischaemia using the Luo-Rudy model [35]. Although the scope of their study was different from ours, they found that the L-type calcium current, rather than the sodium current, determined the occurrence of conduction blocks in the ischaemic core, which is consistent with our results.

We performed additional simulations to investigate which component of ischaemia (hyperkalaemia, acidosis or anoxia) was responsible for the 2:1 conduction block. We repeated separately our simulations for each component. We observed alternating conduction blocks and reentry only in the case of hyperkalaemia. It is the only component of ischaemia that, by its depolarizing effect on the membrane, can suppress the sodium current enough to allow calcium-supported propagation.

Electrical uncoupling has been found to occur during acute myocardial ischaemia [25,26] and to play an important role in the arrhythmogenesis [31]. We found that electrical uncoupling affected slightly the size of the area of conduction block: due to the reduced conductivity, slightly larger portions of the ischaemic BZ exhibited propagation failure on alternate beats. The rate-dependence of the 2:1 conduction block remained, however, unaffected.

Ventricular arrhythmias occur in two distinct phases after the onset of ischaemia [4–6]. The first phase, called immediate arrhythmias by Kaplinsky et al. [5] or phase 1a arrhythmias [27], occurs between 2 and 10 min after coronary occlusion. After a relative arrhythmia-free interval, a second peak, referred to as phase 1b [27], lasts from 15 to 45 min of ischaemia. In our study we used parameter values typical of 10–15 min ischaemia [23], which could be associated with late phase 1a arrhythmias or early phase 1b arrhythmias. Incorporating electrical uncoupling, which is typically involved in the phase 1b arrhythmias [31], did not substantially affect the result of our simulations. Most important for the mechanism described in this study is the presence of a non-conductive ischaemic core surrounded by a border zone of highly depressed excitability in which conduction is mostly supported by the calcium current.

Limitations

Our computational model used an idealized rectangular geometry for the ischaemic region. However, it provides some basic insights in the arrhythmogenesis during acute regional ischaemia. The observed 2:1 conduction blocks depend on the local availability of the calcium current and they are therefore likely to occur for different and more complex geometries as well. Different shapes of the area exhibiting alternating conduction block might, however, affect the subsequent formation of reentry and its dynamics.

The size of the border zone in the intramural direction (about 1 cm) was based on experimental results [21,36]. In the transmural direction, studies of myocardial infarction have reported the existence of a surviving epicardial layer. The thickness of this layer varied from 500 μm [37] up to 3 mm [38]. In our model, the transmural distance between the ischaemic core and the epicardium is about 3 mm, which lies within the reported range. Since the arrhythmogenesis starts at the intramural (lateral) interface between the ischaemic and normal tissue, we believe, however, that our results will also hold for thinner surviving epicardial layers.

Conclusion

We discovered that, at sufficiently high frequencies of excitation, a thin layer surrounding the ischaemic core shows alternating patterns of propagation with 2:1 conduction block. Although the conduction blocks occurred in a small region around the ischaemic core, they caused APD alternans throughout a large portion of the slab of cardiac tissue, leading to T-wave alternans and reentry. Interestingly, during acute regional ischaemia, APD and T-wave alternans developed secondary to the conduction blocks, which provides a novel mechanism for ischaemia-related arrhythmias and their link with APD alternans.

Acknowledgment

The authors would like to thank Dr. S. Pandit, Dr. A. Zaitsev and Dr. E. Tolkacheva for valuable discussions and C. Danko for careful reading of this manuscript. This research was supported by NIH grants 5RO1HL071635 and 5RO1HL071762 and NSF grant CTS-0319555.

References

[1] Davies MJ. Pathological view of sudden cardiac death. Br Heart J 1981;45:88—96.

[2] Goldstein S, Landis JR, Leighton R, Ritter G, Vasu CM, Lantis A, et al. Characteristics of the resuscitated out-of-hospital cardiac arrest victim with coronary heart disease. Circulation 1981;64:977—84.

[3] Zipes DP, Wellens HJ. Sudden cardiac death. Circulation 1998;98:2334—51.

[4] Janse MJ, Wit AL. Electrophysiological mechanisms of ventricular arrhythmias resulting from myocardial ischemia and infarction. Physiol Rev 1989;69:1049—169.

[5] Kaplinsky E, Ogawa S, Balke CW, Dreifus LS. Two periods of early ventricular arrhythmia in the canine acute myocardial infarction model. Circulation 1979;60:397—403.

[6] Menken U, Wiegand V, Bucher P, Meesmann W. Prophylaxis of ventricular fibrillation after acute experimental coronary occlusion by chronic beta-adrenoceptor blockade with atenolol. Cardiovasc Res 1979;13:588—94.

[7] Kurz RW, Mohabir R, Ren XL, Franz MR. Ischaemia induced alternans of action potential duration in the intact-heart: dependence on coronary flow, preload and cycle length. Eur Heart J 1993;14:1410—20.

[8] Nearing BD, Verrier RL. Progressive increases in complexity of T-wave oscillations herald ischemia-induced ventricular fibrillation. Circ Res 2002;91:727—32.

[9] Dilly SG, Lab MJ. Electrophysiological alternans and restitution during acute regional ischaemia in myocardium of anaesthetized pig. J Physiol 1988;402:315—33.

[10] Arce H, Xu A, Gonzalez H, Guevara MR. Alternans and higher-order rhythms in an ionic model of a sheet of ischemic ventricular muscle. Chaos 2000;10:411—26.

[11] Arce H, Lopez A, Guevara MR. Triggered alternans in an ionic model of ischemic cardiac ventricular muscle. Chaos 2002;12:807—18.

[12] Pastore JM, Girouard SD, Laurita KR, Akar FG, Rosenbaum DS. Mechanism linking T-wave alternans to the genesis of cardiac fibrillation. Circulation 1999;99:1385—94.

[13] Pham Q, Quan KJ, Rosenbaum DS. T-wave alternans: marker, mechanism, and methodology for predicting sudden cardiac death. J Electrocardiol 2003;36(Suppl.):75—81.

[14] Smith JM, Clancy EA, Valeri CR, Ruskin JN, Cohen RJ. Electrical alternans and cardiac electrical instability. Circulation 1988;77:110—21.

[15] Hoffman BF, Suckling EE. Effect of heart rate on cardiac membrane potentials and the unipolar electrogram. Am J Physiol 1954;179:123—30.

[16] Kleinfeld M, Magin J, Stein E. Electrical alternans in single ventricular fibers of the frog heart. Am J Physiol 1956;187:139—42.

[17] Fox JJ, Riccio ML, Hua F, Bodenschatz E, Gilmour Jr RF. Spatiotemporal transition to conduction block in canine ventricle. Circ Res 2002;90:289—96.

[18] Qu Z, Garfinkel A, Chen PS, Weiss JN. Mechanisms of discordant alternans and induction of reentry in simulated cardiac tissue. Circulation 2000;102:1664—70.

[19] Coronel R, Wilms-Schopman FJ, Dekker LR, Janse MJ. Heterogeneities in $[K+]_o$ and TQ potential and the inducibility of ventricular fibrillation during acute regional ischemia in the isolated perfused porcine heart. Circulation 1995;92:120—9.

[20] Kleber AG, Janse MJ, Wilms-Schopmann FJ, Wilde AA, Coronel R. Changes in conduction velocity during acute ischemia in ventricular myocardium of the isolated porcine heart. Circulation 1986;73:189—98.

[21] Coronel R, Fiolet JW, Wilms-Schopman FJ, Schaapherder AF, Johnson TA, Gettes LS, et al. Distribution of extracellular potassium and its relation to electrophysiologic changes during acute myocardial ischemia in the isolated perfused porcine heart. Circulation 1988;77:1125—38.

[22] Faber GM, Rudy Y. Action potential and contractility changes in Na(+)(i) overloaded cardiac myocytes: a simulation study. Biophys J 2000;78:2392—404.

[23] Shaw RM, Rudy Y. Electrophysiologic effects of acute myocardial ischemia: a theoretical study of altered cell excitability and action potential duration. Cardiovasc Res 1997;35:256—72.

[24] Panfilov AV, Keener JP. Reentry in three-dimensional myocardium with twisted anisotropy. Physica D 1995;84:545—52.

[25] Kleber AG, Riegger CB, Janse MJ. Electrical uncoupling and increase of extracellular resistance after induction of ischemia in isolated, arterially perfused rabbit papillary muscle. Circ Res 1987;61:271—9.

[26] Riegger CB, Alperovich G, Kleber AG. Effect of oxygen withdrawal on active and passive electrical properties of arterially perfused rabbit ventricular muscle. Circ Res 1989;64:532—41.

[27] Rush S, Larsen H. A practical algorithm for solving dynamic membrane equations. IEEE Trans Biomed Eng 1978;25:389—92.

[28] Zaritsky RM, Pertsov AM. Simulation of 2-D spiral wave interactions on a Pentium-based cluster. In: Proceedings of neural, parallel, and scientific computations. Atlanta; GA, USA: Dynamic Publishers; 2002. p. 187—90.

[29] Walker ML, Rosenbaum DS. Repolarization alternans: implications for the mechanism and prevention of sudden cardiac death. Cardiovasc Res 2003;57:599—614.

[30] Shaw RM, Rudy Y. Electrophysiologic effects of acute myocardial ischemia. A mechanistic investigation of action potential conduction and conduction failure. Circ Res 1997;80:124—38.

[31] De Groot JR, Coronel R. Acute ischemia-induced gap junctional uncoupling and arrhythmogenesis. Cardiovasc Res 2004;62:323—34.

[32] Downar E, Janse MJ, Durrer D. The effect of acute coronary artery occlusion on subepicardial transmembrane potentials in the intact porcine heart. Circulation 1977;56:217—24.

[33] Smith JM, Cohen RJ. Simple finite-element model accounts for wide range of cardiac dysrhythmias. Proc Natl Acad Sci U S A 1984;81:233—7.

[34] Wang Y, Rudy Y. Action potential propagation in inhomogeneous cardiac tissue: safety factor considerations and ionic mechanism. Am J Physiol Heart Circ Physiol 2000;278:H1019—29.

[35] Ferrero JM, Trenor B, Rodriguez B, Saiz J. Electrical activity and reentry during acute regional ischemia: insights from simulations. Int J Bif Chaos 2003;13:3703—15.

[36] Janse MJ, Cinca J, Morena H, Fiolet JW, Kleber AG, de Vries GP, et al. The ''border zone'' in myocardial ischemia. An electrophysiological, metabolic, and histochemical correlation in the pig heart. Circ Res 1979;44:576—88.

[37] Peters NS, Coromilas J, Severs NJ, Wit AL. Disturbed connexin43 gap junction distribution correlates with the location of reentrant circuits in the epicardial border zone of healing canine infarcts that cause ventricular tachycardia. Circulation 1997;95:988—96.

[38] Cardinal R, Vermeulen M, Shenasa M, Roberge F, Page P, Helie F, et al. Anisotropic conduction and functional dissociation of ischemic tissue during reentrant ventricular tachycardia in canine myocardial infarction. Circulation 1988;77:1162—76.